Attractive Osmotic Pressure in an Electric Double Layer with Grafted Polyelectrolytes

J. Ennis,* L. Sjöström,† T. Åkesson,‡ and Bo Jönsson§

Physical Chemistry 2, Chemical Center, P.O. Box 124, S-221 00 Lund, Sweden

Received: June 5, 1997; In Final Form: September 15, 1997

The double-layer interaction between one wall neutralized by both grafted polyelectrolytes and mobile counterions and another wall neutralized only by mobile counterions can give rise to an attractive osmotic pressure. This has been previously observed in both experiments and Monte Carlo simulations. Here a simplified model of this system is studied, in which the polyelectrolyte is replaced by "grafted" ions which interact with the grafting wall via a one-dimensional potential. In a mean field approximation, the model can be solved numerically, and certain cases are analytically tractable. The accuracy of the mean field approximation is tested by Monte Carlo simulations. Regardless of the exact form of the grafting potential, the simplified model proves to have the same qualitative features as simulations of the more complicated system where the configurations of the polyelectrolyte chains are explicitly included. In particular, in the absence of salt the interaction is repulsive at long-range but can be strongly attractive at medium-range, depending on the proportion of grafted ions and the width of the grafting potential. The interaction is again repulsive at short-range. The most interesting result is that addition of sufficient salt always causes the interaction to become attractive at long-range, primarily due to the change in the ideal contribution to the pressure.

1. Introduction

The interaction between two macroions immersed in an electrolyte solution is normally dominated by strong repulsive forces.[1,2] The repulsion has its origin in the overlap of the diffuse double layers of counterions neutralizing the charged particles. There is also an attractive force component due to correlations between counterions, and this turns out to be the dominating one in many systems with divalent counterions, or elsewhere when the ion−ion interaction is strong. This has been clearly shown in simulations and anisotropic hypernetted chain calculations.[3−5]

Addition of neutral salt to an electric double layer normally leads to a decreased repulsion; that is, the macroion−macroion interaction becomes exponentially screened. In a double layer with divalent counterions or where the added salt contains divalent counterions it is possible to have a change from repulsion to attraction or vice versa,[6,7] and the situation can be summarized as a delicate balance between attractive and repulsive forces, generally with a very weak *net* force.

Instead of single multivalent ions, one can consider a salt containing chain molecules with charged groups, i.e. polyelectrolytes. These are quite common in colloidal systems both in nature and in technical applications and usually have a profound influence on colloid stability. Let us initially consider a salt-free system, where polyelectrolytes act as counterions to two infinite charged planar walls. The polyelectrolytes consist of monomers of the opposite charge to the walls, and the chains are free to move in the intervening space. The repulsive double-layer interaction seen with monovalent counterions will completely disappear under these conditions, and the polyelectrolytes will instead give rise to a strong short-ranged attraction.[8] The attraction is due to the polyelectrolytes bridging from one charged wall to the other, resulting in an elastic stretching of the chains. The electrostatic repulsion between the chains forces them to reside close to the charged walls; this is the energetically most favorable configuration. The chain entropy, however, is very low under these conditions. Thus, by bridging from one charged wall to the other one, the chain gains substantial entropy. On the other hand, a monomer in the midregion contributes much more to the electrostatic energy than one at the wall, which means that the bridging can involve only a few monomers. The attraction will be strong but short-ranged and of importance only when the surface−surface separation is of the same order as the monomer−monomer separation. Therefore it will be essentially independent of chain length. For separations larger than the monomer−monomer distance the interaction will be virtually zero and much smaller than the ordinary double−layer repulsion, and so not detectable by a surface force experiment.[9]

Whether the chains are free or grafted with one end to either of the two walls is immaterial, as also is the detailed description of the bonding potential between the monomers of the chain. The attraction will increase with surface charge density, and the minimum in the force−distance curve will become deeper and narrower at the same time as it is shifted inward. This behavior is qualitatively described in the polyelectrolyte mean field theory due to Podgornik.[10,11]

In a recent publication[12] we have shown that additional attractive mechanisms may appear in double-layer systems containing polyelectrolytes as counterions. Imagine a system consisting of two charged walls, where one wall carries grafted neutralizing counterions and where the second wall is neutralized by mobile small counterions. The second wall could also be neutralized by free (nongrafted) polyelectrolytes. The asymmetry will cause an imbalance in charge and there will appear

* Corresponding author. E-mail: fk2jek@beckmann.fkem2.lth.se.
† fk2lsm@beckmann.fkem2.lth.se.
‡ fk2tor@grosz.fkem2.lth.se.
§ fk2boj@grosz.fkem2.lth.se.

S1089-5647(97)01853-1 CCC: $15.00
Published on Web 03/03/1998

a very long-ranged attraction. The effect has been observed experimentally in a number of different systems, but has not been fully understood.[13−16]

Numerical simulations are powerful tools for investigating different models and approximations, but they are time-consuming and at the end only produce a number. The mean field approach can provide a more genuine feeling for the physical mechanisms and is in this respect superior to numerical simulations. The development of double-layer theory in the last 15 years has shown that the mean field approximation is quite reasonable for systems with monovalent ions, but can be qualitatively incorrect when divalent ions are present.

Previous mean field theories of polyelectrolytes at interfaces can be roughly divided into four main groups. For the purposes of comparison with the approach used in this paper, we shall summarize the main features of these theories and refer to some representative works. In all cases the electrostatic potential is treated via the Poisson−Boltzmann equation with the polyelectrolyte monomers as an additional charged species. The differences center on the description of the monomer distribution, and since the latter is coupled to the electric field, this usually results in a set of equations that must be solved self-consistently. All the theories are to some extent based upon previous work on neutral polymers, and in the absence of the external field they give essentially Gaussian statistics for the polyelectrolyte chains i.e. long-range electrostatic correlations within the chain are ignored.

The first group of theories treat the chain conformations via a step-weighted lattice model.[17−22] The problem is generally treated as a first-order Markov process, so that the monomer distributions can be easily generated from a recurrence relation. Alternatively, for end-grafted polyelectrolytes Monte Carlo (MC) simulation can be used to sample self-avoiding walks on the lattice.[23] Flory−Huggins parameters χ can be used to model the nonelectrostatic interactions between different species, and the finite volume of segments can be taken into account by introducing a constraint on the occupation of the lattice sites. Refinements of the model include titrating groups on the polyelectrolye,[19] varying dielectric constants, and finite ion size.[20] The advantage of lattice models is that the discreteness of charge and the finite length of the polyelectrolyte are retained. The discrete nature of the lattice should be a significant drawback only at small surface separations or where the potential varies rapidly on the scale of the lattice spacing.

In the second group of theories, the conformations of the chain are represented as the solution of a diffusion equation with an excluded volume term and an external electrostatic potential.[10−11,24−27] This can be viewed as a continuum limit of the lattice model just described. The diffusion equation can then be solved by using an eigenfunction expansion and assuming ground-state dominance, which is appropriate for very long chains. This treatment can take account of equilibrium with the polyelectrolye in bulk and short-range surface interactions.[27] The assumption of a continuous charge distribution along the chain should be reasonable on length scales much greater than the typical charge−charge separation.

The third kind of theory, dubbed the polyelectrolyte Poisson−Boltzmann (PPB), allows for Boltzmann weighting of the bonding potentials between adjacent monomers and the grafting potential between the wall and one end of the chain.[8,28,29] Thus it resembles the theories of the first group, with a discrete charge distribution along the chain and a finite chain length, but with a continuous distribution of bond lengths and orientations rather than using a lattice, and no excluded volume term. In these respects it is particularly convenient for comparisons with Monte Carlo simulations of strong polyelectrolytes, but the absence of the excluded volume term makes it less applicable for weakly charged polyelectrolytes.

The fourth group of theories are for the particular case of polyelectrolytes adsorbed on neutral surfaces or surfaces with charge of the same sign, where the adsorbed layer is typically very extended.[30−34] The monomers interact with each other through the mean field of the monomer density and through the electrostatic potential. The monomer density is then determined self-consistently, using an analogy from classical mechanics. This approach is valid for moderately high grafting densities and weak excluded volume interactions, but less accurate at very low surface coverage, when the mean field is weak, and at very high surface coverage, when the excluded volume effect is no longer proportional to the monomer density.

In this communication we construct a highly simplified model for the asymmetric polyelectrolyte system described above. When the electrostatics are treated in the mean field approximation, this approach is equivalent to PPB (the third kind of theory listed above) for a chain of length 1, but with an "effective" grafting potential. Alternatively it can viewed as a generalization of a model used by Hesselink for studying adsorption of polyelectrolytes.[35] At the mean field level our model is essentially an ansatz for the functional form of the monomer distribution in the case of strongly charged polyelectrolytes on a surface of opposite charge. This ansatz greatly simplifies the mathematical treatment, since we are left with the Poisson−Boltzmann equation plus a normalization condition for the density of the grafted chains. For some specialized cases we can solve the mean field equations, and in the more difficult cases we can at least provide asymptotic solutions. The accuracy of the mean field approximation for our asymmetric model system is tested against MC simulations of a few cases using the same model. Comparisons are also done with MC simulations of a system with explicit chains, in which it is demonstrated that the simplified model has the right qualitative features and for suitable choices of the "effective" grafting potential can give semiquantitative agreement with the simulations over a range of conditions.

Our general result is that a salt-free double layer which has an intrinsic asymmetry can give rise to a net attractive osmotic pressure, although it will always be asymptotically repulsive. The addition of salt will increase the attraction, and the asymptotic repulsion found in salt-free solutions will in many cases be replaced by an attraction.

2. Model

In simulation work, a polyelectrolyte is often represented by hard charged spherical beads connected by harmonic springs. This has the advantage of avoiding the complications of angle-dependent potentials, while still retaining the main features of the structure. The ions are also represented by charged hard spheres, the solvent enters only via the dielectric constant, and the solid surfaces are represented as infinite plane walls with uniform surface charge density. A representation of this kind of model is given in Figure 1, and some results from MC simulations on it are given in this paper.

Now consider a model in which the monomers in the polyelectrolyte have been replaced by ions that are each grafted to a charged wall by a specified one-dimensional grafting potential; that is, in addition to their Coulombic interactions with other ions and the charged walls, they are subject to a nonelectrostatic grafting force, which depends only on the

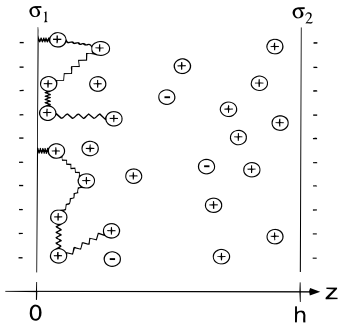

Figure 1. Schematic picture of a model system for the interaction between one charged wall at $z = 0$ neutralized by grafted polyelectrolytes, represented by hard spheres and harmonic springs, and another charged wall at $z = h$ neutralized by mobile counterions. The system may also be in equilibrium with a bulk salt solution.

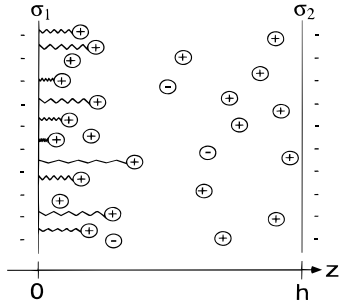

Figure 2. Schematic picture of a simplified model system for the interaction between one charged wall at $z = 0$ neutralized by grafted ions, represented by hard spheres for the ions and springs for the grafting potential, and another charged wall at $z = h$ neutralized by mobile counterions. The system may also be in equilibrium with a bulk salt solution.

distance from the grafting wall and which only acts in the direction normal to the wall. This grafting force is such that the grafted ions are effectively trapped within a finite distance of that wall. There are no bonds with other ions. Thus the chain length of the polyelectrolyte has been discarded, and the constraints of chain connectivity have been replaced by the grafting potential. Here we take advantage of the fact that highly charged polyelectrolytes grafted to surfaces of opposite charge at low salt concentrations adopt fairly flat conformations, and the resulting interaction is found to be insensitive to chain length. This phenomenon was first analyzed for neutral chains grafted to a "sticky" wall[36,37] and for other cases with attractive potentials.[38,39] For a sufficiently attractive interaction the thickness of the adsorbed layer is finite for long chains and the profile is exponentially decaying. This effect was also observed in various theories of adsorbed polyelectrolytes[8,18,25] and deduced from various experimental measurements.[9,40−42]

We shall assume that the amount of polyelectrolyte per unit surface area is given and remains fixed as the separation varies. Thus in our simplified model we do not determine the adsorbed amount nor allow equilibrium with a bulk polyelectrolyte solution. The model could be extended along the lines of Hesselink's calculation[35] to include a nonelectrostatic adsorption energy per monomer, which would then balance the electrostatic free energy to give the equilibrium adsorption at each separation. However this complicates the analysis further and so will not be attempted here.

Figure 2 gives a schematic representation of the simplified model. A version of this model has been introduced earlier[12] and analyzed via a mean field simulation. Here we explore the model more fully in the mean field approximation and obtain analytic results in some special cases.

Let the grafted ions have valence υ_g and local number density $n_g(z)$, where z is the distance from the wall with the grafted ions. Let the valencies and number densities of the mobile ions be denoted by υ_+ and $n_+(z)$ for the cations and υ_- and $n_-(z)$ for the anions. We shall assume a symmetric electrolyte (where salt is present), and we primarily have in mind a 1:1 electrolyte since the mean field approximation is known to be reasonable for monovalent ions. Furthermore, we shall assume that the grafting ions are cations and that they have the same valence as the mobile cations. Denote by h the separation of the two walls, and denote by γ the proportion of the surface charge of the grafting wall that is neutralized by the grafting ions. In the absence of salt, we must have $0 \le \gamma \le 1$, whereas in the presence of salt we only need $\gamma \ge 0$. However our model is not suitable for polyelectrolyte brushes, which adopt more extended conformations, so the region of validity is limited to γ not much greater than 1. The charge density on the grafting surface will be denoted by σ_1 and on the other wall by σ_2.

The grafting potential shall be denoted by $V(X)$, where V is in units of k_BT and $X = z/d$, where the grafting surface is at $X = 0$ and d is the characteristic width of the grafting potential, i.e. $V(X=1) \sim O(1)$. We shall primarily consider two special cases for the form of $V(X)$. The first is

$$V(X) = 0 \quad \text{for} \quad X < 1$$
$$= \infty \quad \text{for} \quad X \ge 1 \tag{1}$$

so that the grafted ions are restricted to $z < d$. We shall refer to this as the "confined" case.

The second special case is

$$V(X) = X^2 \tag{2}$$

which we shall refer to as the "harmonic" case.

The electrostatic potential $\bar{\psi}(z)$ satisfies Poisson's equation

$$\nabla^2\bar{\psi} = -\frac{4\pi}{\epsilon}\rho(z) \tag{3}$$

where $\rho(z)$ is the charge density at z and ϵ is the dielectric permittivity, which in SI units equals $4\pi\epsilon_0\epsilon_r$, where ϵ_0 is the permittivity of free space and ϵ_r is the relative permittivity of the solvent.

Using the mean field approximation and taking account of the symmetry, eq 3 becomes

$$\frac{d^2\bar{\psi}}{dz^2} = -\frac{4\pi e}{\epsilon}(\upsilon_+ n_+^\infty \exp(-e\upsilon_+\bar{\psi}/(k_BT)) + \upsilon_- n_-^\infty \exp(-e\upsilon_-\bar{\psi}/(k_BT)) + \upsilon_g n_g^\infty \exp(-e\upsilon_g\bar{\psi}/(k_BT) - V(z/d))) \tag{4}$$

where e is the elementary charge and n_+^∞ and n_-^∞ are the concentrations of the respective species at the point where $\bar{\psi}$ is taken to be zero. It is clear from this equation that at the mean field level our simplified model is equivalent to an ansatz for the functional form of the monomer density profile.

Where there is salt present, it is natural to take the zero of potential to be out in the bulk solution, so that $n_+^\infty = n_-^\infty = n$, where n is the salt concentration in bulk. When only counterions are present, then $n_-^\infty = 0$, and the zero of potential may be taken for convenience at the location of the potential minimum. The number density n_g^∞ is a parameter that is determined in the course of the solution. As discussed above, we shall assume

that $v = v_g = v_+ = -v_-$. For the grafted ions, we have the constraint

$$\int_0^h v e n_g(z)\, dz = -\gamma\sigma_1 \tag{5}$$

For the boundary conditions on $\bar{\psi}$, we shall assume that the dielectric constant of the wall is negligible, so that

$$\left.\frac{d\bar{\psi}}{dz}\right|_{z=0} = -\frac{4\pi\sigma_1}{\epsilon}$$

$$\left.\frac{d\bar{\psi}}{dz}\right|_{z=h} = \frac{4\pi\sigma_2}{\epsilon} \tag{6}$$

In the mean field approximation, the net osmotic pressure between the two walls, P, can be split into physically relevant components at a particular location $z = m$ as follows:

$$P = P^{id} + P^{asym} + P^{bridge} \tag{7}$$

Here, P^{id} is the ideal component of the pressure. P^{asym} is due to the asymmetry of the charge distribution in the subsystems and is given by $-2\pi\sigma_s^2/\epsilon$, where σ_s is the net charge per unit area on the subsystem $z < m$. P^{bridge} is the average of the total grafting force per unit area on grafted ions for $z > m$, i.e. ions whose grafting "bonds" cross $z = m$. This will be attractive if $V(X)$ is a nondecreasing function of X. If one goes beyond mean field, there are two additional contributions to P, due to electrostatic correlations and core−core correlations across $z = m$, and these are computed in the MC simulations that we use to check the validity of the mean field approximation.

We define a dimensionless potential ψ by

$$\psi = -\frac{ev\bar{\psi}}{k_B T} \tag{8}$$

In the salt-free case, it is convenient to define a dimensionless surface charge by

$$s_i = -\frac{4\pi\sigma_i e v d}{\epsilon k_B T} \geq 0 \quad \text{for} \quad i = 1,2 \tag{9}$$

while in the salt case it is more natural to define it by

$$S_i = -\frac{4\pi\sigma_i v e}{\epsilon\kappa k_B T} \quad \text{for} \quad i = 1,2 \tag{10}$$

where

$$\kappa^2 = \frac{8\pi n e^2 v^2}{\epsilon k_B T} \tag{11}$$

3. Analysis

3.1. Semianalytic Solutions: "Confined" Case. When the grafting potential $V(X)$ has the form given in eq 1, then we can obtain a semianalytic solution valid for all values of the separation, surface charge, etc. By semianalytic we mean that the solution depends on parameters that are given implicitly as the solutions to nonlinear transcendental equations. Since the resulting equations are not particularly transparent and there are a number of cases to consider, all details have been confined to Appendices A and B. Some insight can then be gained by an analysis of these equations in the limit of large separation, and this we consider in sections 3.2 and 3.3. In general though, one needs to solve the equations numerically, just as one must do for the usual nonlinear Poisson−Boltzmann equation for finite separations. Results of this kind are given in section 4.

3.2. Large Separations: Counterions Only. If the separation h is made large, while other parameters are fixed, then our asymptotic results for the osmotic pressure between the two walls can be written in the form

$$P = \frac{\epsilon(k_B T)^2}{2\pi e^2 v^2 h^2} C_0\left(1 - A_1\frac{d}{h} + O\left(\left(\frac{d}{h}\right)^2\right)\right) \tag{12}$$

where C_0 is found by solving the usual mean field equations for counterions only and with the charge on the grafting wall reduced by a factor $1 - \gamma$. The equations for C_0 and its asymptotic behavior are given in Appendix C. Most importantly, C_0 goes to a numerical constant as $h \to \infty$ (see eqs 112 and 113). Thus asymptotically the pressure between the walls is always repulsive at large enough separations and decays as h^{-2} with a coefficient independent of the surface charge densities and the properties of the grafted ions (except that it has different values in the cases $s_1(1 - \gamma) = 0$ and $s_1(1 - \gamma) > 0$). The first correction that depends on the details of the surfaces is at $O(h^{-3})$.

Expressions for the coefficient A_1 in eq 12 for various forms of the grafting potential are given in Appendix C (see eqs 114, 117, and 120). For the confined case A_1 is positive, so the presence of the grafted layer always makes the net pressure less repulsive. If $\gamma = 1$, then A_1 is proportional to s_1 for large s_1 (see eq 116), so the net pressure can become attractive when $d/h \sim 1/s_1$. When $\gamma < 1$, then A_1 is bounded as $s_1 \to \infty$ (see eq 119), and this bound is $O(1)$ unless γ is quite close to 1. Thus in a sense $\gamma = 1$ is an anomalous case, since for $\gamma < 1$ the net pressure can only become attractive when the confining distance is an appreciable fraction of the wall-to-wall separation.

For a fairly general grafting potential $V(X)$ we can obtain an expression for A_1 for low s_1 (see eq 120). Here the effect of the grafted layer is again to make the net pressure less repulsive, regardless of the form of $V(X)$. Thus at low surface charge the effects on the coefficient A_1 found in the confined case are general and are not sensitive to the form of $V(X)$. Were it not so, then the whole approach would be of questionable use, since the grafting potential $V(X)$ is only a crude way of modeling the tendency of the polyelectrolyte to adopt flat conformations when adsorbed at the surface. Although we do not have an expression for A_1 valid for general s_1 and a general grafting potential $V(X)$, numerical evidence indicates that the results are qualitatively the same as in the confined case.

3.3. Large Separations: Salt. When salt is included, the asymptotic form of the pressure between the two walls can be obtained from analyzing the decay of the electrostatic potential ψ near an isolated wall in contact with the same bulk salt concentration. For the primitive model double layer in a planar geometry, it has been shown from asymptotic analysis[43] that at large distances z from an isolated wall the electrostatic potential will decay as

$$\psi \sim S^* \exp(-\kappa z) \tag{13}$$

where κ is a property of the bulk electrolyte and S^* is a scaled effective surface charge. In general this κ is not equal to the Debye κ given by eq 11 except in the limit of low concentrations,[44] but at the mean field level of approximation they are equal. The constant S^* depends both on the properties of the bulk electrolyte and also on properties of the surface. The

pressure between two walls at large separations h is then given by

$$P \sim 4k_B T n S_1^* S_2^* (-\kappa h) \tag{14}$$

where S_1^* and S_2^* are the scaled effective surface charges of the two walls.

If one now includes the grafted ions, then the above analysis still holds as long as $\exp(-V(X))$ is nonzero over a strictly finite range, e.g. the confined case. When $\exp(-V(X))$ is not of finite range the analysis should be valid as long as $V(X)/X$ increases faster than some positive power of X as $X \to \infty$.

In what follows we shall use eq 13 as our definition of an effective surface charge at the mean field level, with κ given in eq 11.

In our system, the effective surface charge for the wall without grafted ions is given at the mean field level by

$$S_2^* = \frac{8}{S_2}((1 + S_2^2/4)^{1/2} - 1) \tag{15}$$

For small S_2 we have $S_2^* = S_2 - S_2^3/16 + O(S_2^5)$, while for $S_2 \to \infty$ we have $S_2^* \to 4$.

The effective surface charge for the wall with the grafted ions, S_1^*, is not as simple, but we can obtain analytic results in various cases. For the confined potential we obtain two coupled nonlinear equations in two unknowns (taking $C \to -2$ in Appendix B). Even then, the solution must still be found numerically, and examples of this will be given in section 4. Some progress can be made by considering the case when $S_1^* = 0$. Since S_2^* is always positive, then if S_1^* changes from positive to negative, the pressure between the two surfaces changes from repulsive to attractive at long-range (see eq 14). We shall refer to the change of sign of S_1^* as a "charge reversal". If we fix $S_1^* = 0$ and take $S_1 \to \infty$, then we obtain a single nonlinear equation (eq 127 in Appendix D) relating κd and γ at the point of charge reversal. These results indicate that for a given value of κd, there is a critical value of γ at which charge reversal occurs and above which the pressure becomes attractive. This critical γ value is always less than 1 and is monotonically decreasing as κd increases (see Figure 9). The full numerical solution is discussed in section 4.

For a general grafting potential $V(X)$, arbitrary κd, and arbitrary surface charge densities, only numerical solutions for S_1^* are available, and these are also considered in section 4. However for small κd we can obtain a solution by asymptotic matching (eq 131). The most important observation is that the first effect of the grafting layer for small κd is always to decrease S_1^*, regardless of the precise form of $V(X)$. The critical value of γ (at which $S_1^* = 0$) is less than 1, and it decreases as κd increases. As in the case with counterions only, the behavior of the system is not sensitive to the form of $V(X)$.

In the case when the surface potentials are low, we can also obtain the following expression for S_1^* for a general form of the grafting potential:

$$S_1^* = S_1\left(1 - \frac{\gamma \int_0^\infty \cosh(\kappa d X)\exp(-V(X))\,dX}{\int_0^\infty \exp(-V(X))\,dX}\right) + O(S_1^2) \tag{16}$$

If $\gamma > 0$, then S_1^* decreases monotonically without bound as κd increases, while as $\kappa d \to 0$, $S_1^* \to S_1(1 - \gamma)$. This suggests that we can always obtain a long-range attraction in our system if the width of the grafting potential is large enough relative to the Debye length.

3.4. Monte Carlo Simulations. The MC simulations were performed in the canonical ensemble with the traditional Metropolis algorithm.[45] Due to the symmetry of the model system, periodic boundary conditions are used in the lateral directions. Within the simulation box each ion interacts with all other particles, including the charged walls, according to the minimum image convention. Since the electrostatic interactions are long-ranged, the effect of charges outside the box has to be taken into account. This contribution is considered as an external potential, numerically determined from the average charge distribution within the box; further details are found elsewhere.[46,47]

In this simulation work four different models are considered. In the first one the system consists only of counterions of two kinds. One of the species is free to move in the whole system, while the other one is confined to a region close to the left-hand wall. In the second system one of the walls is (partly) neutralized by grafted chains made up of 10 charged monomers. In these two models the ions are represented as point particles. In the third case we add a symmetric electrolyte to the first system, and in the fourth case we likewise add a symmetric electrolyte to the second system. In these last two systems a hard core diameter of 4.25 Å is used for all species and only monovalent ions are considered. The hard wall constraints and the confinement constraint are applied in relation to the center of each particle; for example, for the hard walls, the position of the centers is restricted to $0 < z < h$.

The pair interaction between two monovalent charges i and j, separated by a distance r_{ij}, is given by

$$u_{el}(r_{ij}) = \frac{e^2}{\epsilon r_{ij}} \qquad r_{ij} > d$$

$$u_{hc}(r_{ij}) = \infty \qquad r_{ij} \le d \tag{17}$$

In addition, two connected monomers interact with a harmonic potential:

$$u_h(r_{ij}) = K r_{ij}^2 \tag{18}$$

where K is the force constant. To graft the chains to the walls, the same harmonic potential is used. Instead of using the constant K, we refer to r_{min}, defined as

$$r_{min} = \left(\frac{e^2}{2\epsilon K}\right)^{1/3} \tag{19}$$

In all the simulations in this paper $r_{min} = 5$ Å. The Monte Carlo (MC) simulations were in most cases carried out with around 160 counterions, and in some cases up to 40 salt ions were added. At least 30 000 configurations per particle were used to equilibrate the system, and the production runs were more than 7 times as large. The effect of the MC-box size on calculated number was checked by simulations with twice as many particles, and no significant differences were observed.

In the presence of salt, the equilibrium with the bulk is determined by the chemical potential, which is obtained by a modified Widom's technique developed for electrolyte systems.[48] Since the net pressure is obtained as the difference between the pressure in the double layer and in the bulk, which roughly are of the same size, a high precision is needed for these numbers in order to obtain accurate results. The chemical potentials must also be determined accurately in order to

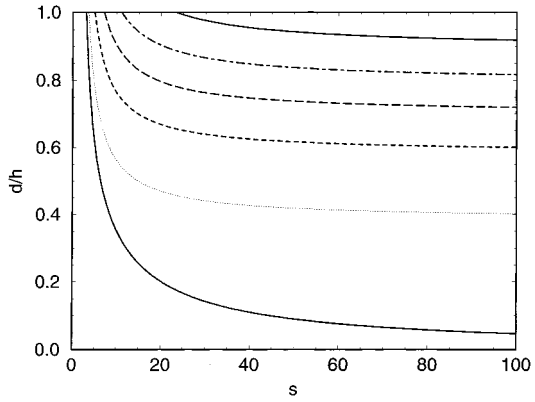

Figure 3. Crossover between attraction and repulsion for counterions only in the confined case. s is the scaled surface charge density. For a given value of γ the region below the corresponding curve corresponds to repulsion and the region above the curve but below $d = h$ corresponds to attraction. For $d > h$ the net pressure is always repulsive. Lower solid line: $\gamma = 1$. Dotted: $\gamma = 0.9$. Short dashes: $\gamma = 0.7$. Long dashes: $\gamma = 0.5$. Dot−dash: $\gamma = 0.3$. Upper solid line: $\gamma = 0.1$

determine a correct bulk density. In these simulations five "ghost" particles were inserted at least every 100 configurations.

4. Results and Discussion

4.1. Counterions Only. As discussed in section 3.1, in the confined case the solution of the mean field equations can be expressed in terms of two parameters that satisfy two coupled nonlinear equations, given in Appendix A. These can be tackled by Newton−Raphson iteration, using the asymptotic estimates in section 3.2 and Appendix C to provide a good initial estimate at large separations.

The analysis in section 3.2 implies that we may find a region of net attraction as the separation varies, especially if $\gamma \approx 1$ and $s_1 \gg 1$. This is confirmed by Figure 3 for the case where both walls have the same bare charge density. The curve for each value of γ indicates where the net pressure is zero, with repulsion occurring for parameters below the curve (at larger separations) and attraction occurring above it. Note that at $d = h$ there is a jump discontinuity in the pressure, as the confining region coincides with the opposite wall. For $h < d$ the confinement has no effect, and the mean field equations correspond to a normal system with counterions only, for which the net pressure is always repulsive. Thus there is another crossover from attraction to repulsion at $d = h$.

Figure 3 shows that the region of attraction may be quite large at $\gamma = 1$, but shrinks rapidly as γ falls below 1. When $s_1 = s_2 = s$ and $s \rightarrow \infty$, the critical value of d/h below which the net pressure is always repulsive is given for $\gamma = 1$ by the hyperbolic curve

$$\frac{\pi^2}{2s} \tag{20}$$

and for $\gamma < 1$ by the constant asymptote

$$\frac{x}{1+x} \tag{21}$$

where

$$x = \left(\frac{1-\gamma}{\gamma}\right)^{1/2}\left(\frac{\pi}{2} + \arctan\left(\left(\frac{1-\gamma}{\gamma}\right)^{1/2}\right)\right) \tag{22}$$

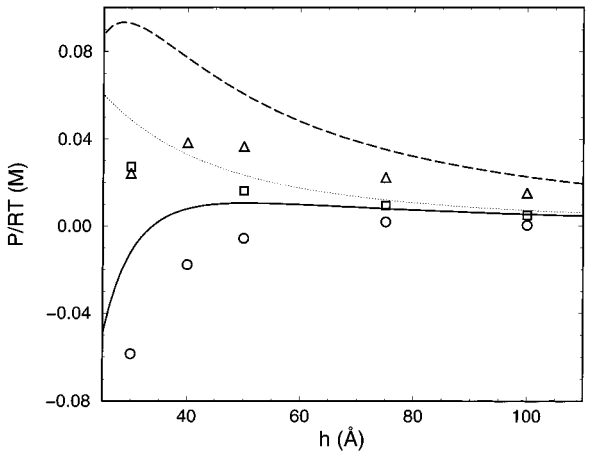

Figure 4. Comparison of mean field results with Monte Carlo simulations in the confined case, giving the net osmotic pressure P as a function of the separation h while fixing the confining distance d at 10 Å. The lines are the mean field results, and the symbols are the MC points. Solid line and circles: $\gamma = 1$, surface charge density 71.4 Å^2 per charge. Dotted line and squares: $\gamma = 1$, 285.6 Å^2 per charge. Dashed line and triangles: $\gamma = 0.9$, 71.4 Å^2 per charge.

This is in accord with the results in Appendix C, where the coefficient of the h^{-3} term increases as s for large s when $\gamma = 1$, but approaches a constant for large s when $\gamma < 1$.

It is also evident in Figure 3 that there is a minimum value of s below which the net pressure is repulsive at all separations. This critical value of s is given by

$$s_{\text{scrit}} = 4\left(\frac{2}{\gamma} - 1\right)^{1/2} \arctan\left(\left(\frac{2}{\gamma} - 1\right)^{1/2}\right) \tag{23}$$

and increases rapidly when γ is small. Since s_1 is proportional to $\sigma_1 d$ (eq 9), by fixing h and σ_1 and increasing d, it is always possible to obtain an attraction in the mean field approximation if $\gamma > 0$.

The validity of the mean field approximation for the confined case can be checked by comparison to Monte Carlo simulations. Since only counterions are present, it is sufficient to use point ions. The pressure is computed at the midplane, and if $d/h < 0.5$, then there is no contribution from bridging. In all the simulations in this paper we use $T = 298.0$ K and a relative dielectric permittivity of 78.7, which we shall refer to as the "standard" conditions. Figure 4 shows the comparison for $d = 10$ Å and various values of h, the different curves being for two values of γ (0.9 and 1.0) and two values of the surface charge density (71.4 and 285.6 Å^2 per elementary charge). The MC pressures are more attractive than the mean field results, particularly at shorter separations when the electrostatic correlation contribution to the pressure becomes significant. Nevertheless the qualitative features remain the same. At $\gamma = 1$ and 71.4 Å^2 per charge there is a long-range repulsion, which soon crosses over to an attraction at shorter range. If we lower γ to 0.9, then the pressure becomes more repulsive. Similarly if we keep $\gamma = 1$ and lower the surface charge density to 285.6 Å^2 per charge, then the net pressure also becomes repulsive. Note that this latter value of the surface charge is below the critical value given from eq 23, and so the mean field pressure is repulsive at all separations.

A further comparison is shown in Figure 5 for $h = 100$ Å and varying d, the different curves again being for two values of γ (0.9 and 1.0) and two values of the surface charge density (71.4 and 285.6 Å^2 per elementary charge). The agreement with the MC pressures improves as d increases. The qualitative

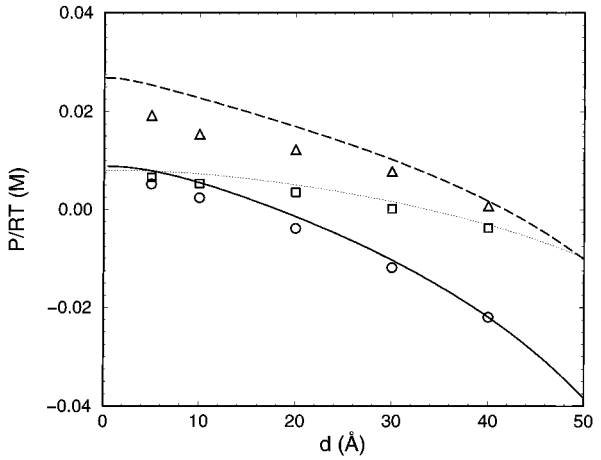

Figure 5. Comparison of mean field results with Monte Carlo simulations in the confined case, giving the net osmotic pressure P as a function of the confining distance d while fixing the separation h at 100 Å. The lines are the mean field results, and the symbols are the MC points. Solid line and circles: $\gamma = 1$, surface charge density 71.4 Å^2 per charge. Dotted line and squares: $\gamma = 1$, 285.6 Å^2 per charge. Dashed line and triangles: $\gamma = 0.9$, 71.4 Å^2 per charge.

features of the mean field results are again confirmed by the MC results. The region of attraction is much reduced if γ drops below 1 or the surface charge density is lowered. As $d \rightarrow 0$, then the mean field result tends to that for counterions only, with the charge on the grafted wall reduced by a factor of $1 - \gamma$, and so if $\gamma = 1$, then the limiting value of the pressure is independent of σ_1. However in the simulations, when $d \rightarrow 0$, then the point ions are confined to the surface, so even for $\gamma = 1$ the pressure depends on σ_1 and is in general more attractive than the equivalent system with mobile counterions only.

We can obtain some insight into the mechanism behind the long-range attraction by examining the components of the pressure at some location between the walls. For convenience we use the midplane, although it is obviously not a plane of symmetry of the system. The confined case has the disadvantage that there is a jump discontinuity in the bridging contribution to the pressure when the confining surface coincides with the plane at which we are considering components. Thus we instead focus on the harmonic case, when $V(X) = X^2$. To do this we solve eq 4 numerically, using the Bulirsch−Stoer method and a shooting technique (with Newton−Raphson iteration) to satisfy the two boundary conditions (eq 6) and the charge balance constraint eq 5. The latter is best evaluated at the same time as taking a Bulirsch−Stoer step, since this obviates the need for additional storage and allows rational function extrapolation to be used for the integration as well.

Figure 6 shows the midplane components for $d = 20$ Å, $\gamma = 1$, and a surface charge density of 71.4 Å^2 per charge (for our "standard" ϵ and T) and varying h. For $h > 150$ Å the net pressure is repulsive, with the ideal contribution dominating over the asymmetric term and the bridging term being negligible. Since we have $\gamma = 1$, the only mobile counterions are those that neutralize the right-hand wall. At these large separations the relatively thin layer of grafted ions has little effect on the distribution of these mobile counterions, and the system closely resembles one with an uncharged wall and a charged wall neutralized by counterions only. For $h > 150$ Å the net pressure becomes attractive, initially with the asymmetric term in the pressure slightly dominating the ideal term. Now the layer of grafted ions has begun to affect the distribution of mobile counterions, causing more of them to be present in the grafted layer than would otherwise be the case.

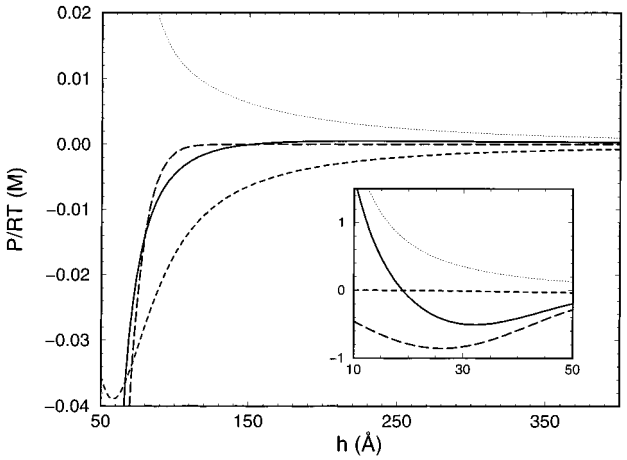

Figure 6. Components of the net pressure at the midplane for the harmonic case as a function of the separation h. $d = 20$ Å, $\gamma = 1$, and the surface charge density is 71.4 Å^2 per charge ($s = 25.08$). Solid line: net pressure P. Dotted: P^{id}. Short dashes: P^{asym}. Long dashes: P^{bridge}.

As h decreases further, the bridging term begins to dominate (see the inset in Figure 6), as the harmonically grafted ions begin to penetrate into the right-hand side of the system. Correspondingly, the charge asymmetry of the system has decreased, and so the asymmetric component of the pressure plays a lesser role. At short separations ($h < 18$ Å), the grafted ions are less affected by the grafting potential, so the bridging contribution is now decreasing in magnitude, the asymmetric term is very small, and the ideal term dominates, giving a net repulsion again.

It is not initially obvious what causes the excess accumulation of mobile ions in the grafted layer, which leads to the attraction discussed above. We have explored this matter further by quantifying the contributions to the free energy within the mean field approximation. We find that the accumulation is in some cases driven by the entropy of the ions but more often by a gain in energy. We can analyze the process in two steps defined as follows: let us start from ion distributions obtained in systems with only one charged wall. The grafted ions interact with a charged wall to the left, while the mobile ions see a charged wall to the right. The two species do not interact with each other, and the initial distributions are simply obtained as a superposition of the independent distributions. We then turn on the interactions and let the mobile ions respond to the fixed distribution of grafted ions and the second charged wall, which is equivalent to an interaction with an external field. In the next step the grafted ions, as well as the mobile ones, are allowed to respond, and the final distributions obtained after this process correspond to the completely relaxed solution.

In the first step, at intermediate separations, for low surface charge densities or for rather dense charge distributions of the grafted ions, the dominating contribution to the free energy change stems from the entropy of the mobile ions. The increase of entropy is caused by a flow of ions from regions with locally high concentrations into the layer close to the left-hand wall. On the other hand, in systems where the excess entropy of the mobile ions is low, which corresponds to a situation where the ion distribution has a more pronounced nonuniformity, this flow of ions could result in a small increase, or even a loss of entropy. Under such circumstances the process is driven by energy, which is also the case in systems where the grafted ions are distributed over a larger volume. A mobile ion that enters the layer of grafted ions "sees" a nonzero surface charge and is therefore attracted to the left-hand wall.

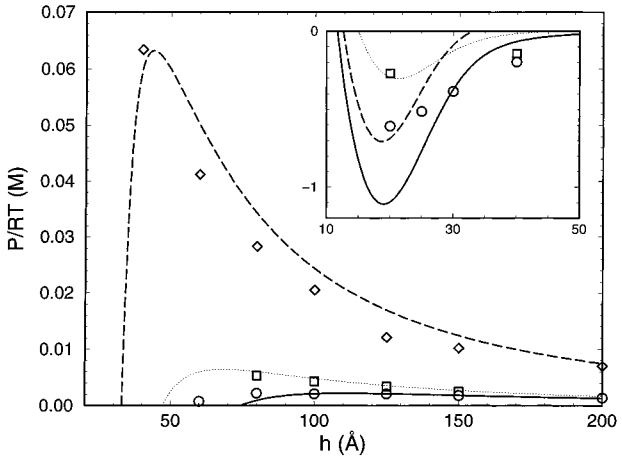

Figure 7. Comparison between Monte Carlo simulation with decamers and the mean field solution of the simplified model with the harmonic grafting potential and $d = 11.5$ Å. The net osmotic pressure is given as a function of separation h for various values of γ and σ. The symbols are the MC results, and the lines are the simplified model. Solid line and circles: $\gamma = 1.0$, one charge per 50.77 Å. Dotted line and squares: $\gamma = 1.0$, one charge per 101.54 Å^2. Long dashes and diamonds: $\gamma = 0.875$, one charge per 50.77 Å^2.

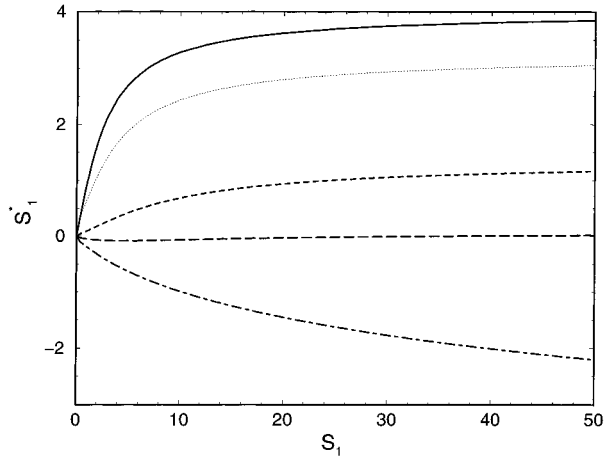

Figure 8. Effective surface charge density as a function of the actual surface charge density, both in dimensionless units (see text), for $\kappa d = 1$ and a range of γ values. Solid line: $\gamma = 0.0$. Dots: $\gamma = 0.4$. Short dashes: $\gamma = 0.8$. Long dashes: $\gamma = 0.9$. Dot−dash: $\gamma = 1.0$.

During the final step, the distribution of the grafted ions becomes more extended, which causes an additional flow of mobile ions into the grafted layer. The repulsion between the two species increases, and the process leads to a state of higher energy. This is however compensated for by an increase in the entropy of the grafted ions.

The utility of our highly simplified model has been tested by comparison with Monte Carlo simulations on a system with chain molecules, here of length 10. In Figure 7 the results for three different sets of parameters are given, one with $\gamma = 1$ and a surface charge density of one charge per 50.77 Å^2, a second with $\gamma = 0.875$ and the same charge density, and a third with $\gamma = 1$ and a charge density of one charge per 101.54 Å^2. The numerical results from our simplified model use a harmonic grafting potential with $d = 11.5$ Å, chosen to fit the simulation results in the first case for $h > 80$ Å (since our model should be best at representing the large separation behavior rather than the bridging regime). The same value of d is then used for the other two cases.

The agreement between the two approaches is semiquantitative in the large separation regime and qualitative in the bridging regime (the inset in Figure 7). This indicates that our simplified model has captured the dominant physical effects in the more complex system. The fact that a fixed value of d gives good agreement even when γ and σ_1 are varied suggests that it is more than a fitting parameter; that is, it captures some of the constraints on the monomers due to the chain connectivity. Thus d should depend strongly on r_{min} (i.e., on the force constant for the monomer−monomer interaction) and weakly on γ and σ_1.

4.2. Salt. As discussed in section 3.3, when salt is present, the interaction at large separations can be analyzed in terms of the effective surface charges of each surface. Since S_2^* is always positive if the right-hand wall is charged, the sign of the net pressure at large separations is the same as that of S_1^*, as follows from eq 14.

Figure 8 shows the effective surface charge density for the wall with grafted ions as a function of the actual surface charge density S_1, using the dimensionless variables defined in eqs 10 and 13. The uppermost curve, for $\gamma = 0$, shows how in the absence of any grafted ions the effective surface charge density increases monotonically and saturates as the real surface charge density increases. As γ is increased, the maximum value of S^* slowly decreases. Then for $0.904 > \gamma > 0.851$, S^* first decreases slightly and then increases slightly as S increases. Thus in this narrow range of parameters the pressure at large separations is weakly attractive at low surface charge density and becomes weakly repulsive as the surface charge density increases. For $\gamma > 0.904$, S^* is negative and monotonically decreasing; that is, the net pressure between the two surfaces is attractive whatever the magnitude of the surface charge density, and the saturation is slow.

Thus in this case for γ close to 1 the wall with the grafted ions interacts with the other wall as though its surface charge density was of opposite sign of the actual bare charge. This is a charge-reversal phenomenon, similar to that which has been observed in double layers with multivalent counterions.[43] The electrostatic potential near the wall changes sign within the grafted layer, corresponding to the fact that the accumulated net charge from the grafted ions and the mobile counterions and co-ions overcompensates the bare charge on the grafting wall. Since this effect is present in a mean field calculation, it is clearly not due (in this situation) to ion−ion correlations. The mechanism behind the charge reversal is best viewed as the combination of two effects. Firstly the introduction of the grafting potential causes the grafted ions to reside close to that wall. Secondly, the mobile counterions entering the grafted layer "see" more of the bare surface charge, and so for primarily energetic reasons the number density of these ions is larger than it would be were the grafted ions collapsed onto the grafting wall. Correspondingly the number density of the mobile co-ions is reduced just near the wall. The net charge accumulated near the grafting wall can now exceed the bare surface charge density, and a charge reversal occurs. As we shall see, this explanation accords with the fact that the effect is sensitive to both properties of the grafted ions (e.g. d, the width of the grafting potential) and salt concentration.

We saw from Figure 8 that increasing γ at fixed κd can lead to a charge reversal. Figure 9 shows the location of the point of charge reversal, $S_1^* = 0$, as a function of both κd and γ for the confined and the harmonic cases. In the harmonic case the horizontal axis is $\kappa d(3/2)^{1/2}$, chosen to give agreement at low S_1 and low κd (using the analytic results in Appendix D and eq 16), in order to demonstrate the effective similarity of the two grafting potentials. For each case curves are shown for low surface charge density (these are analytic results; see eq 16)

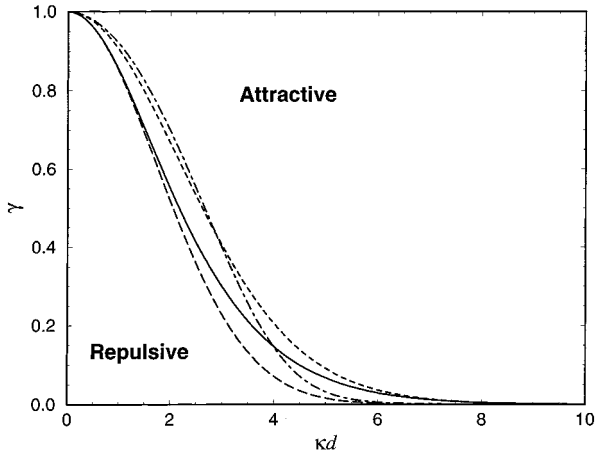

Figure 9. Asymptotic cross-over between repulsion and attraction in the presence of salt. For parameters in the region below the corresponding curve the net pressure is repulsive at large separations, and above it attractive. In the harmonic case the horizontal axis is scaled as $\kappa d(3/2)^{1/2}$. Solid line: confined case, low S_1 limit. Short dashes: confined case, large S_1 limit. Long dashes: harmonic case, low S_1 limit. Dot−dash: harmonic case, $S_1 = 50$.

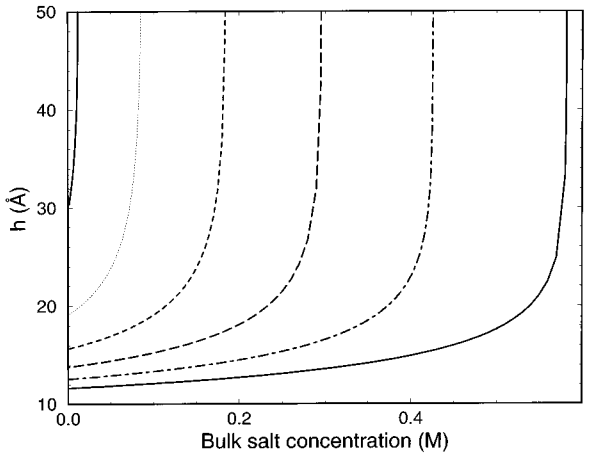

Figure 10. Crossover between repulsion and attraction in the confined case at finite separation in the presence of salt, as a function of salt concentration and separation h (in Å). The surface charge density is one charge per 71.4 Å^2, and $d = 10$ Å. For parameters in the region below the corresponding curve but with $h > 10$ Å the net pressure is attractive, and above the curve it is repulsive. Solid line at left: $\gamma = 0.99$. Dots: $\gamma = 0.9$. Short dashes: $\gamma = 0.8$. Long dashes: $\gamma = 0.7$. Dot−dash: $\gamma = 0.6$. Solid line at right: $\gamma = 0.5$.

and high surface charge density (this is semianalytic for the confined case and numerical for the harmonic case). It is clear that the variation of surface charge density has only a weak effect on the location of the $S_1^* = 0$ line. With the indicated rescaling of the horizontal axis it is clear that the confined and harmonic cases have qualitatively the same behavior. In both cases the value of γ needed to give $S_1^* = 0$ is monotonically decreasing as κd increases. It is clear that by increasing the bulk salt concentration and so increasing κ while keeping the other parameters fixed, we can always move the system into the attraction regime at large separations if $\gamma > 0$. The same effect can be obtained by increasing γ with other parameters fixed, but this is physically more difficult to achieve.

The above conclusion is only strictly valid at large separations. To illustrate this point in more detail, we examine the location of the attractive/repulsive crossover in the confined case at finite separations, which can be investigated semianalytically. Figure 10 shows the crossover for $d = 10$ Å and a surface charge density of one charge per 71.4 Å^2, as a function of salt concentration and separation. Here the net pressure is repulsive above the curve for the corresponding γ value and then attractive in the parameter region between the curve and $h = 10$ Å (if $h < d$, then in the confined case and the mean field approximation for $\sigma_1 = \sigma_2$ the net pressure is always repulsive, since the bridging contribution is zero and the asymmetric contribution is zero at the midplane). We see that for $h > d$ and $\gamma > 0$ we can always obtain an attractive pressure by increasing the salt concentration while keeping the other parameters fixed. Note however that this mean field result may involve quite high salt concentrations if γ is low, and in this regime the additional pressure contributions which are neglected in the mean field may become important.

There is an interesting difference between the results for the pressure with counterions only and the results with salt present. For counterions only the pressure is always repulsive at long-range, whereas in the presence of salt the pressure may be attractive at long-range. Clearly, at fixed separation it must be possible to pass between these cases by changing the salt concentration, and this should give us some more insight into the underlying mechanism. Figure 11 shows the components of the net pressure at the midplane for $h = 50$ Å, $d = 10$ Å, a surface charge density of one charge per 71.4 Å^2, and $\gamma = 1$.

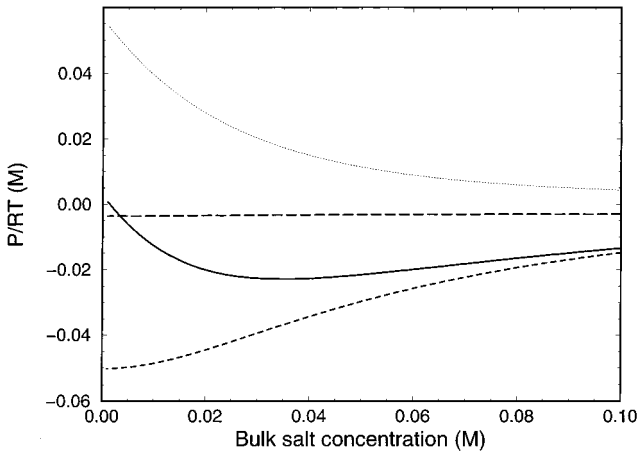

Figure 11. Components of the net pressure at the midplane between surfaces for the harmonic grafting potential as a function of salt concentration. The surface charge density is one charge per 71.4 Å^2, $h = 50$ Å, $d = 10$ Å, and $\gamma = 1$. Solid line: net osmotic pressure P. Dots: P^{id}. Short dashes: P^{asym}. Long dashes: P^{bridge}.

The bridging contribution is quite insensitive to salt concentration. At low salt concentrations the change in the net pressure from repulsion to attraction is driven by the changes in P^{id}. Even if the ion distributions between the walls are much the same when a small amount of salt is added to the system, nevertheless increasing the bulk concentration must still cause a decrease in the ideal term and thus in the net pressure, and this is the major component of the change at low concentrations. As more salt is added, there is also a screening of the asymmetric term and the ideal term, with the former remaining dominant.

The accuracy of the mean field approximation in the presence of salt can again be tested by comparing with Monte Carlo simulations using the same model. Figure 12 shows the comparison for the confined case with $\gamma = 0.8$, $d = 10$ Å, $h = 30$ Å, and a surface charge density of one charge per 71.4 Å^2. The MC points give somewhat more attractive pressures, but the qualitative trend is the same. In particular, the addition of monovalent salt causes the net pressure to become attractive.

The utility of our highly simplified model can be tested by comparison with Monte Carlo simulations on an equivalent

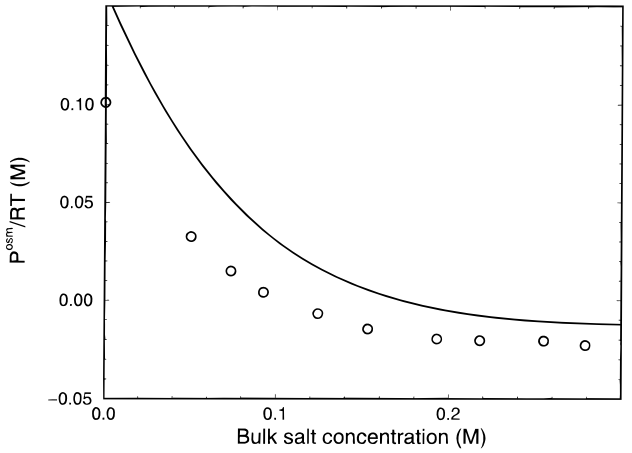

Figure 12. Comparison of mean field results with Monte Carlo simulations in the confined case with added salt, giving the net osmotic pressure P^{osm} as a function of the bulk salt concentration. $d = 10$ Å, $h = 30$ Å, $\gamma = 0.8$, and the surface charge density is one charge per 71.4 Å. The solid line is the mean field result, and the circles are the MC points.

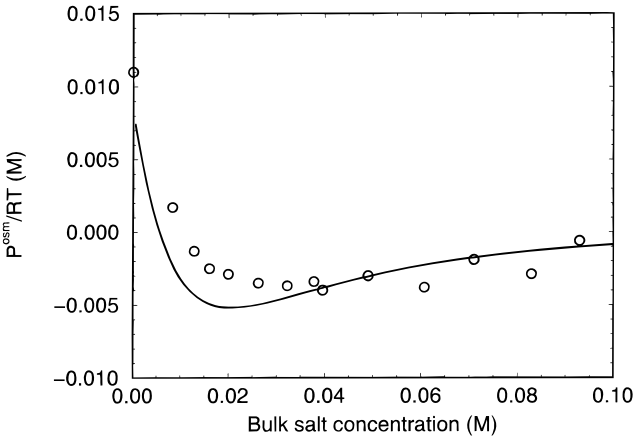

Figure 13. Comparison of mean field results with Monte Carlo simulations using decamers, in the presence of added salt. $\gamma = 0.9877$, $h = 80$ Å, and the surface charge density is one charge per 50.77 Å^2. The mean field results use a harmonic grafting potential with $d = 11.5$ Å. The solid line is the mean-field result, and the circles are the MC points.

system with chain molecules. Figure 13 shows the results for $\gamma = 0.9877$, $h = 80$ Å, and a charge density of one charge per 50.77 Å^2. The mean field results are for the harmonic case with $d = 11.5$ Å, the same value used in the mean field results in Figure 7 and chosen there to fit the large separation results for $\gamma = 1$. The agreement here is again better than qualitative and confirms that the addition of monovalent salt can cause the net pressure to become attractive. It also shows that the simplified model has some predictive power using a *fixed* value of d while varying other system parameters.

The theoretical prediction of long-range attractions in this asymmetric system in the presence of salt is in qualitative agreement with experimental observations. As a contribution to the theory of surface forces, our simplified model is an interesting variation on the standard mean field treatment of the electrical double layer, since by restricting some of the ions it is possible to obtain an attraction. In the context of colloidal dispersions, the presence of a long-range attraction will make the dispersion unstable. To this end, the required asymmetry could be produced in various ways, e.g by adding polyelectrolyte to only one part of the system or by mixing dispersions containing different kinds of particles.

5. Conclusions

In this paper we have explored the behavior of what is effectively a two-parameter model of a polyelectrolyte grafted to a surface of opposite charge. To avoid the complexities of explicitly considering chain conformations, the polyelectrolyte is replaced by ions that interact with the grafting wall via a nonelectrostatic potential that depends only on the distance from the wall. The two parameters are the proportion of the bare surface charge density neutralized by the grafted ions, γ, and the width of the grafting potential, d. We have then used this representation to consider the interaction in an asymmetric system in which one wall is (partly) neutralized by the grafted ions and the other wall is neutralized only by mobile counterions.

The obvious advantage of our simplified model is that in the mean field approximation it is readily treated either analytically (in various limits) or numerically. The validity of the mean field approach itself has been checked against selected MC simulations and found to be quantitatively reasonable and qualitatively correct. Despite the simplifications, our model also qualitatively reproduces the main features found in simulations, which include the chain conformations explicitly, independent of the precise form of the grafting potential $V(X)$ that we use in the simplified model. Thus we have a clearer picture of the interactions that occur in such asymmetric systems and the mechanisms that lie behind them. This is particularly useful for the case when salt is present and at large separations, as here simulations are more difficult to perform.

When only counterions and grafted ions are present, the pressure will always be repulsive at large enough separations. At intermediate separations the pressure may become attractive if the surface charge density is above a critical value. This effect is most pronounced when $\gamma = 1$; at lower values of γ it only occurs when h/d is $O(1)$. The driving force is the accumulation of mobile counterions in the grafted layer (in excess of what would be found if the grafted ions were collapsed onto the wall).

When salt is added to the system, the pressure may also become attractive at long-range on the scale of the Debye length. This can be made to occur either by increasing γ or increasing κd and can be achieved by the addition of sufficient salt. This long-range attraction is perhaps the most novel feature of our analysis and is due to a "charge reversal" near the wall with the grafted ions, which arises from the accumulation of mobile counterions there.

Appendix A: Confined Case, Counterions Only

In the analysis of the salt-free case it is convenient to define the following dimensionless quantities:

$$\delta = \frac{d}{h} \tag{24}$$

$$y = \frac{z}{h} \tag{25}$$

$$\alpha = \frac{2\pi e^2 \upsilon^2 n_+^\infty h^2}{\epsilon k_B T} > 0 \tag{26}$$

$$\beta = \frac{2\pi e^2 \upsilon^2 n_g^\infty h^2}{\epsilon k_B T} \geq 0 \tag{27}$$

$$\bar{s}_i = -\frac{4\pi\sigma_i e \upsilon h}{\epsilon k_B T} = \frac{s_i}{\delta} \tag{28}$$

Then the equations become

$$\frac{d^2\psi}{dy^2} = 2\alpha e^{\psi} + 2\beta e^{\psi - V(y/\delta)} \tag{29}$$

$$\left.\frac{d\psi}{dy}\right|_{y=0} = -\bar{s}_1 \tag{30}$$

$$\left.\frac{d\psi}{dy}\right|_{y=1} = s_2 \tag{31}$$

$$2\beta\int_0^1 e^{\psi - V(y/\delta)}\, dy = \gamma\bar{s}_1 \tag{32}$$

Since only counterions are present, some simplifications occur. First note that $\bar{s}_i > 0$ in eq 28. From eqs 30 and 31 it follows that ψ must have a minimum for $0 \le y \le 1$, and from eq 29 it follows that there can only be one such minimum. We choose the zero of the potential to be at this minimum. We shall refer to $y < \delta$ as the "inner" region and $\delta \le y \le 1$ as the "outer" region.

For the "inner" region, we have

$$\frac{d^2\psi}{dy^2} = 2(\alpha + \beta)\exp(\psi) \tag{33}$$

and for the "outer" region,

$$\frac{d^2\psi}{dy^2} = 2\alpha\exp(\psi) \tag{34}$$

In addition, we have the boundary conditions given by eqs 30 and 31, the charge balance condition

$$2\beta\int_0^{\delta}\exp(\psi)\, dy = \gamma\bar{s}_1 \tag{35}$$

and the requirement that ψ and its first derivative are continuous across $y = \delta$ (these conditions are necessary since $V(X)$ has a discontinuity there).

There are three cases to consider: (1) The minimum is in the outer region. (2) The minimum is in the inner region, and the net pressure is repulsive. (3) The minimum is in the inner region, and the net pressure is attractive. In case 1, the net pressure is always repulsive.

Case 1. In the inner region,

$$\psi = \ln[c_2\sec^2((y + c_3)((\alpha + \beta)c_2)^{1/2})] \tag{36}$$

In the outer region,

$$\psi = \ln[\sec^2((y + c_4)(\alpha)^{1/2})] \tag{37}$$

There are five unknowns, c_2, c_3, c_4, α, and β, and five conditions. By manipulating these we obtain

$$c_4 = \frac{1}{\alpha^{1/2}}\arctan\left[\frac{\bar{s}_2}{2\alpha^{1/2}}\right] - 1 \tag{38}$$

$$c_2 = 1 + \frac{\beta}{\alpha + \beta}\tan^2[(\delta + c_4)\alpha^{1/2}] \tag{39}$$

$$c_3 = -\frac{1}{((\alpha + \beta)c_2)^{1/2}}\arctan\left[\frac{\bar{s}_1}{2(c_2(\alpha + \beta))^{1/2}}\right] \tag{40}$$

where α and β satisfy

$$\sec^2[(\delta + c_4)\alpha^{1/2}] = c_2\sec^2[(\delta + c_3)((\alpha + \beta)c_2)^{1/2}] \tag{41}$$

$$\bar{s}_1\left(\gamma - \frac{\beta}{\alpha + \beta}\right) = 2\beta\left(\frac{c_2}{\alpha + \beta}\right)^{1/2}\tan[(\delta + c_3)((\alpha + \beta)c_2)^{1/2}] \tag{42}$$

The osmotic pressure between the two walls is given by

$$P = \alpha\frac{\epsilon(k_BT)^2}{2\pi e^2 v^2 h^2} = n_+^{\infty} \tag{43}$$

Case 2. In the inner region

$$\psi = \ln[\sec^2((y + c_3)((\alpha + \beta))^{1/2})] \tag{44}$$

In the outer region

$$\psi = \ln[-c_2\sec^2((y + c_4)(-c_2\alpha)^{1/2})] \tag{45}$$

where

$$c_2 = \frac{\alpha + \beta}{4\alpha\beta}\bar{s}_1^{\,2}\left(\gamma - \frac{\beta}{\alpha + \beta}\right)^2 - 1 \tag{46}$$

$$c_3 = -\frac{1}{(\alpha + \beta)^{1/2}}\arctan\left(\frac{\bar{s}_1}{2(\alpha + \beta)^{1/2}}\right) \tag{47}$$

$$c_4 = \frac{1}{(-\alpha c_2)^{1/2}}\arctan\left(\frac{\bar{s}_2}{2(-\alpha c_2)^{1/2}}\right) - 1 \tag{48}$$

and α and β satisfy

$$\sec^2((c_3 + \delta)(\alpha + \beta)^{1/2}) = -c_2\sec^2((c_4 + \delta)(-\alpha c_2)^{1/2}) \tag{49}$$

$$\bar{s}_1\left(\gamma - \frac{\beta}{\alpha + \beta}\right) = \frac{2\beta}{(\alpha + \beta)^{1/2}}\tan((c_3 + \delta)(\alpha + \beta)^{1/2}) \tag{50}$$

The osmotic pressure between the two walls is given by

$$P = -\alpha c_2\frac{\epsilon(k_BT)^2}{2\pi e^2 v^2 h^2} \tag{51}$$

Case 3. In the inner region ψ is given by eq 44 and in the outer region by

$$\psi = \ln[c_2\,\mathrm{csch}^2((y + c_4)(c_2\alpha)^{1/2})] \tag{52}$$

where c_2 is given by eq 46, c_3 is given by eq 47,

$$c_4 = -\frac{1}{\sqrt{(\alpha c_2)}}\mathrm{arccoth}\left(\frac{\bar{s}_2}{2\sqrt{(\alpha c_2)}}\right) - 1 \tag{53}$$

and α and β satisfy eq 50 and

$$\sec^2((c_3 + \delta)\sqrt{(\alpha+\beta)}) = c_2\,\mathrm{csch}^2((c_4 + \delta)(\alpha c_2)^{1/2}) \tag{54}$$

The osmotic pressure is given by eq 51.

In practice, one is usually interested in varying the wall−wall separation while keeping the other parameters fixed. The question then arises of which of the above three cases applies at a given separation. It follows from the results in Appendix

C that case 1 holds at large enough separation. Depending on the values of the other parameters, at shorter separations case 2 and then case 3 may apply. It is useful to be able to determine the separations that correspond to the transition between case 1 and case 2 and the transition between case 2 and case 3. Since we are varying the separation h, it is convenient to use the s_i parameters (see eq 9), which do not depend on h.

Transition from Case 1 to Case 2. At this transition the minimum of ψ is at $y = \delta$. The following equations must be satisfied:

$$s_1 = 2\delta\left(\frac{\alpha}{1-\gamma}\right)^{1/2} \tan\left(\delta\left(\frac{\alpha}{1-\gamma}\right)^{1/2}\right) \tag{55}$$

$$s_2 = 2\delta\alpha^{1/2} \tan((1-\delta)\alpha^{1/2}) \tag{56}$$

where only α and δ depend on h, and β can be obtained from

$$\beta = \frac{\alpha\gamma}{1-\gamma} \tag{57}$$

Transition from Case 2 to Case 3. At this transition the osmotic pressure between the two walls is zero. The variables α and δ satisfy

$$\delta = s_1\left(\gamma - \frac{\beta}{\alpha+\beta}\right)\frac{1}{2}\left(\frac{1}{\alpha}+\frac{1}{\beta}\right)^{1/2} \tag{58}$$

$$\left(\frac{\alpha}{\beta}\right)^{1/2} = \tan\left(\delta(\alpha+\beta)^{1/2} - \arctan\left(\frac{s_1}{2\delta(\alpha+\beta)^{1/2}}\right)\right) \tag{59}$$

where β is given by

$$\beta = -\alpha + \frac{\alpha}{1-\alpha(\delta - 1 - 2\delta/s_2)^2} \tag{60}$$

Appendix B: Confined Case, Salt

In the case with salt present, we define the following dimensionless quantities (in addition to those in Appendix A):

$$u = \kappa z \tag{61}$$

$$H = \kappa h \tag{62}$$

$$D = \kappa d \tag{63}$$

$$B = \frac{n_g^\infty}{2n} \tag{64}$$

Then the equations become

$$\frac{d^2\psi}{du^2} = \sinh(\psi) + \mathrm{B}e^{\psi - V(u/D)} \tag{65}$$

$$\left.\frac{d\psi}{du}\right|_{u=0} = -S_1 \tag{66}$$

$$\left.\frac{d\psi}{du}\right|_{u=H} = S_2 \tag{67}$$

$$B\int_0^H e^{\psi - V(u/D)}\, du = \gamma S_1 \tag{68}$$

For the sake of simplicity, we shall assume that both walls have surface charge of the same sign and that the charge on the grafted ions is opposite in sign of the charge on the walls. Then $S_i \geq 0$, and so it follows that ψ has a minimum for $0 \leq u \leq H$. It can be shown by a more extended argument that there is only one such minimum. We shall refer to $0 \leq u \leq D$ as the "inner" region and $D < u \leq H$ as the "outer" region. The solutions in the outer region are equivalent to those between dissimilarly charged surfaces,[49] so we shall give only brief details.

For the inner region,

$$\frac{d^2\psi}{du^2} = \sinh(\psi) + Be^{\psi} \tag{69}$$

and for the outer region

$$\frac{d^2\psi}{du^2} = \sinh(\psi) \tag{70}$$

We have the boundary conditions given by eqs 66 and 67, the charge balance condition

$$B\int_0^D e^{\psi}\, du = \gamma S_1 \tag{71}$$

and the continuity of ψ and its first derivative across $u = D$.

From these we obtain three nonlinear equations in three unknowns. It is convenient to choose the unknowns to be B, $w_d = \exp(-\psi(u = D))$, and $w_h = \exp(-\psi(u = H))$. We can then define

$$C = {S_2}^2 - w_h - \frac{1}{w_h} \tag{72}$$

and the osmotic pressure between the walls is

$$P = -nk_BT(C+2) \tag{73}$$

Thus $C < -2$ corresponds to a repulsion, while $C \geq -2$ corresponds to an attraction.

There are two major cases to consider, depending on whether the minimum of ψ is in the outer region or the inner region, and then subcases depending on the value of C. We define the following auxiliary quantities.

$$p = C - \frac{2B}{w_d} \tag{74}$$

$$a = \frac{1}{2}(-p + (p^2 - 8B - 4)^{1/2}) \tag{75}$$

$$b = \frac{1}{2}(-p - (p^2 - 8B - 4)^{1/2}) \tag{76}$$

$$k_1 = \left(\frac{b}{a}\right)^{1/2} \tag{77}$$

$$w_0 = \exp(-\psi(u{=}0)) = \frac{1}{2}({S_1}^2 - p - (({S_1}^2 - p)^2 - 8B - 4)^{1/2}) \tag{78}$$

Minimum in Outer Region. In this case $C < -2$, so the net pressure is always repulsive.

The three equations are

$$D = \frac{2}{a^{1/2}}(F(\phi_d, k_1) - F(\phi_0, k_1)) \tag{79}$$

$$S_1\gamma = \frac{2B}{ba^{1/2}}\left(F(\phi_d, k_1) - F(\phi_0, k_1) - E(\phi_d, k_1) + E(\phi_0, k_1) - \left(\left(1 - \frac{w_d}{a}\right)\left(\frac{b}{w_d} - 1\right)\right)^{1/2} + \left(\left(1 - \frac{w_0}{a}\right)\left(\frac{b}{w_0} - 1\right)\right)^{1/2}\right) \tag{80}$$

$$H - D = 2k_2^{1/2}(2K(k_2) - F(\phi_h, k_2) - F(\phi_m, k_2)) \tag{81}$$

where

$$\phi_d = \arcsin\left(\left(\frac{w_d}{b}\right)^{1/2}\right) \tag{82}$$

$$\phi_0 = \arcsin\left(\left(\frac{w_0}{b}\right)^{1/2}\right) \tag{83}$$

$$k_2 = \frac{1}{2}(-C - (C^2 - 4)^{1/2}) \tag{84}$$

$$\phi_h = \arcsin\left(\left(\frac{w_h}{k_2}\right)^{1/2}\right) \tag{85}$$

$$\phi_m = \arcsin\left(\left(\frac{w_d}{k_2}\right)^{1/2}\right) \tag{86}$$

$F(\phi, k)$ is the incomplete elliptic integral of the first kind of amplitude ϕ and modulus k, $E(\phi, k)$ is the incomplete elliptic integral of the second kind, and $K(k)$ is the complete elliptic integral of the first kind of modulus k.[50]

Minimum in Inner Region. The first two equations are

$$D = \frac{2}{a^{1/2}}(2K(k_1) - F(\phi_d, k_1) - F(\phi_0, k_1)) \tag{87}$$

$$S_1\gamma = \frac{2B}{ba^{1/2}}\left(2(K(k_1) - E(k_1)) - F(\phi_d, k_1) - F(\phi_0, k_1) + E(\phi_0\, k_1) + E(\phi_d, k_1) + \left(\left(1 - \frac{w_d}{a}\right)\left(\frac{b}{w_d} - 1\right)\right)^{1/2} + \left(\left(1 - \frac{w_0}{a}\right)\left(\frac{b}{w_0} - 1\right)\right)^{1/2}\right) \tag{88}$$

with other quantities defined as before, and where $E(k)$ is the complete elliptic integral of the second kind of modulus k.[50]

The third equation depends on the value of C, and here there are three subcases to consider.

Case 1: $C \geq 2$. Define

$$f = \frac{1}{2}(C + (C^2 - 4)^{1/2}) \tag{89}$$

$$k_2 = \left(1 - \frac{1}{f^2}\right)^{1/2} \tag{90}$$

Since $d\psi/du > 0$ in the outer region we must have $w_h < w_d$.

If $|\ln(w_d)| \geq |\ln(w_h)|$, then the third equation is

$$H - D = \frac{2}{f^{1/2}}(F(\phi_m, k_2) - F(\phi_h, k_2)) \tag{91}$$

where now

$$\phi_m = \arctan((fw_d)^{1/2}) \tag{92}$$

$$\phi_h = \arctan((fw_h)^{1/2}) \tag{93}$$

If $|\ln(w_d)| < |\ln(w_h)|$, then the third equation is

$$H - D = \frac{2}{f^{1/2}}(F(\phi_h, k_2) - F(\phi_m, k_2)) \tag{94}$$

where now

$$\phi_m = \arctan\left(\left(\frac{f}{w_d}\right)^{1/2}\right) \tag{95}$$

$$\phi_h = \arctan\left(\left(\frac{f}{w_h}\right)^{1/2}\right) \tag{96}$$

Case 2: $-2 \leq C \leq 2$. Define

$$k_2 = \left(\frac{1}{2} - \frac{C}{4}\right)^{1/2} \tag{97}$$

$$\phi_m = \arctan\left(\frac{2w_d^{1/2}}{|w_d - 1|}\right) \tag{98}$$

$$\phi_h = \arctan\left(\frac{2w_h^{1/2}}{|w_h - 1|}\right) \tag{99}$$

Again we must have $w_h < w_d$.

If $w_d < 1$, then the third equation is

$$H - D = F(\phi_m, k_2) - F(\phi_h, k_2) \tag{100}$$

If $w_d > 1$ and $w_h > 1$, then the third equation is

$$H - D = F(\phi_h, k_2) - F(\phi_m, k_2) \tag{101}$$

If $w_d > 1$ and $w_h < 1$, then

$$H - D = 2K(k_2) - F(\phi_h, k_2) - F(\phi_m, k_2) \tag{102}$$

Case 3: $C < -2$. Define

$$k_2 = \frac{2}{-C + (C^2 - 4)^{1/2}} \tag{103}$$

If $w_d > 1$, then the third equation is

$$H - D = 2k_2^{1/2}(F(\phi_h, k_2) - F(\phi_m, k_2)) \tag{104}$$

where

$$\phi_m = \arctan\left(\frac{1}{(k_2w_d - 1)^{1/2}}\right) \tag{105}$$

$$\phi_h = \arctan\left(\frac{1}{(k_2w_h - 1)^{1/2}}\right) \tag{106}$$

If $w_d < 1$, then the third equation is

$$H - D = 2k_2^{1/2}(F(\phi_m, k_2) - F(\phi_h, k_2)) \tag{107}$$

where

$$\phi_m = \arctan\left(\frac{1}{(k_2/w_d - 1)^{1/2}}\right) \tag{108}$$

$$\phi_h = \arctan\left(\frac{1}{(k_2/w_h - 1)^{1/2}}\right) \tag{109}$$

Appendix C: Large Separations: Counterions Only

Taking $h \to \infty$ at fixed d, our results for the pressure have the form given in eq 12 where C_0 satisfies

$$2C_0^{1/2} \tan((1 + C_1)C_0^{1/2}) = \bar{s}_2 \tag{110}$$

$$-2C_0^{1/2} \tan(C_1C_0^{1/2}) = \bar{s}_1(1 - \gamma) \tag{111}$$

Define $\bar{s}_n = \bar{s}_1(1 - \gamma)$. If $\bar{s}_n > 0$, then

$$C_0 = \pi^2\left(1 - 4\left(\frac{1}{\bar{s}_n} + \frac{1}{\bar{s}_2}\right) + 12\left(\frac{1}{\bar{s}_n} + \frac{1}{\bar{s}_2}\right)^2 + O\left(\frac{1}{\bar{s}_2^3}, \frac{1}{\bar{s}_n^3}\right)\right) \tag{112}$$

If $\bar{s}_n = 0$, then

$$C_0 = \frac{\pi^2}{4}\left(1 - \frac{4}{\bar{s}_2} + \frac{12}{\bar{s}_2^2} + O\left(\frac{1}{\bar{s}_2^3}\right)\right) \tag{113}$$

Confined Potential. Define $s_n = s_1(1 - \gamma)$. If $s_n = 0$, then analysis of eqs 41 and 42 (the appropriate equations for the large separation regime) gives

$$A_1 = \frac{s_1}{\beta_2} - 2 \tag{114}$$

where $\beta \sim \beta_2\delta^{-2}$ as $\delta \to 0$ and β_2 is given by the transcendental equation

$$s_1 = 2(\beta_2)^{1/2} \tan((\beta_2)^{1/2}) \tag{115}$$

If s_1 becomes large, then

$$A_1 \sim \frac{4s_1 + 16}{\pi^2} - 2 + O\left(\frac{1}{s_1}\right) \tag{116}$$

Thus when $\gamma = 1$, the first correction to the pressure due to the grafted layer is attractive and becomes large as s_1 increases, so that the net pressure can become attractive at an intermediate range.

When $s_n > 0$, then

$$A_1 = \frac{4\gamma\beta_0^2}{s_n(1 - \gamma(1 + \beta_0^2))} - 2 \tag{117}$$

where β_0 satisfies

$$\beta_0 = \tan\left(-\frac{s_1}{2\beta_0}(1 - \gamma(1 + \beta_0^2)) + \arctan\left(\frac{\beta_0}{1 - \gamma(1 + \beta_0^2)}\right)\right) \tag{118}$$

and $\beta \sim (\pi/\beta_0)^2$ as $\delta \to 0$. If s_1 becomes large, then A_1 is given by

$$A_1 \sim \frac{2\left(\frac{\gamma}{1 - \gamma}\right)^{1/2}}{\arctan\left(\left(\frac{\gamma}{1 - \gamma}\right)^{1/2}\right)} - 2 + O\left(\frac{1}{s_1}\right) \tag{119}$$

Even if s_1 is large, A_1 is $O(1)$ unless γ is close to 1. Thus for $\gamma < 1$ there is a critical value of δ below which the pressure is always repulsive regardless of the surface charge densities.

As $\gamma \to 1$ and so $s_n \to 0$, then there is a crossover between eqs 117 and 114, but since eq 12 contains terms in $1/s_n$, this crossover occurs at infinite separation.

General Grafting Potential. By using the technique of matched asymptotic expansions, we can obtain an expression for A_1 that is valid for low s_1 and fairly general grafting potentials. For the result to be valid, it is sufficient that $V(X)/X \to \infty$ faster than a positive power of X. The result is

$$A_1 = s_1\frac{\gamma M_2}{M_0} - 2s_1^2\gamma(d_0 + d_1\gamma) + O(s_1^3) \tag{120}$$

where

$$M_n = \int_0^\infty X^n \exp(-V(X))\, dX \tag{121}$$

$$d_0 = \frac{2M_3}{3M_0} - \frac{M_2M_1}{2M_0^2} \tag{122}$$

$$d_1 = \frac{M_2M_1}{M_0^2} - \frac{2M_3}{3M_0} - \frac{M_2J_{1,0}}{M_0^3} - \frac{J_{2,1}}{M_0^2} + \frac{2J_{3,0}}{3M_0^2} \tag{123}$$

$$J_{n,m} = \int_0^\infty X^n \exp(-V(X))\, dX \int_X^\infty u^m \exp(-V(u))\, du \tag{124}$$

In the special case of $V(X) = X^2$, the harmonic potential, then we obtain

$$A_1 = \frac{s_1\gamma}{2} + s_1^2\frac{\gamma(14\gamma - 2^{1/2}5)}{6(2\pi)^{1/2}} + O(s_1^3) \tag{125}$$

By comparison, for the confined potential, we obtain

$$A_1 = \frac{s_1\gamma}{3} + s_1^2\frac{\gamma(16\gamma - 15)}{90} + O(s_1^3) \tag{126}$$

which agrees with the low s_1 expansion of eq 117.

Thus the results for a general grafting potential $V(X)$ have the same qualitative features as the confined case discussed in the previous section. For low s_1, the first effect of the grafted ions at $O(h^{-3})$ is always to make the net pressure less repulsive.

Appendix D: Large Separations: Salt

Equation 13 defines an effective surface charge S^*, which can be used in eq 14 to give the pressure between the walls at large separations. We now give some analytic results for S_1^*.

Confined Case. Taking $h \rightarrow \infty$ and fixing $S_1^* = 0$ while taking $S_1 \rightarrow \infty$, we obtain

$$D = 2(1-\gamma)^{1/2}K((1-\gamma)^{1/2}) \tag{127}$$

$$B = \frac{\gamma}{2(1-\gamma)} \tag{128}$$

where $K(k)$ is the complete elliptic integral of the first kind of modulus k.[50] Then

$$\gamma = 1 - \left(\frac{D}{\pi}\right)^2 + \frac{1}{2}\left(\frac{D}{\pi}\right)^4 - \frac{5}{32}\left(\frac{D}{\pi}\right)^6 + O(D^8) \quad \text{for} \quad D \ll 1 \tag{129}$$

$$\approx 16\exp(-D) \quad \text{for} \quad D \gg 1 \tag{130}$$

General Grafting Potential. Define $S_n = S_1(1-\gamma)$. Then for $D \ll 1$, the method of matched asymptotic expansions gives

$$S_1^* = \frac{8}{S_n}((1+S_n^2/4)^{1/2} - 1) - D^2\frac{S_1P_2\gamma(1+S_n^2/2)}{(1+S_n^2/4+(1+S_n^2/4)^{1/2})} - D^3\frac{S_1^2\gamma}{(1+S_n^2/4+(1+S_n^2/4)^{1/2})}(P_3(1+S_n^2/2) + P_4S_n(1+S_n^2/4)^{1/2}) + O(D^4) \tag{131}$$

$$P_2 = \frac{M_2}{M_0} \tag{132}$$

$$P_3 = \frac{1}{M_0^2}(M_2M_1 + M_3M_0 + \gamma(J_{2,1} - J_{3,0} - 2M_2J_{0,1}/M_0 - M_3M_0)) \tag{133}$$

$$P_4 = \frac{1}{3M_0^2}(-M_3M_0 + \gamma(3J_{2,1} - J_{3,0} + M_3M_0)) \tag{134}$$

where the moment integrals M_n are defined in eq 121 and the double integrals $J_{n,m}$ in eq 124. Since the moment integrals are positive irrespective of the form of the grafting potential, the term involving D^2 is always negative. If γ is close to 1 and so S_n is small, then the second term can dominate, so that S_1^* is negative.

For the harmonic case we obtain

$$P_2 = \frac{1}{2} \tag{135}$$

$$P_3 = \frac{1}{\pi^{1/2}}\left(\frac{3}{2} + \gamma\left(\frac{1}{2^{1/2}2} - 2\right)\right) \tag{136}$$

$$P_4 = -\frac{1}{3\pi^{1/2}}(1 - \gamma 2^{1/2}) \tag{137}$$

For the confined case we obtain

$$P_2 = \frac{1}{3} \tag{138}$$

$$P_3 = \frac{5}{12} - \frac{41\gamma}{90} \tag{139}$$

$$P_4 = -\frac{1}{12} + \frac{2\gamma}{15} \tag{140}$$

Note that in eq 131, for large S_1, the coefficient of D^2 scales as S_1, and the coefficient of D^3 scales as S_1^2. Thus eq 131 is only valid for $S_1 \ll 1/D$.

References and Notes

(1) Derjaguin, B. V.; Landau, L. *Acta Phys. Chim. URSS* **1941**, *14*, 633.
(2) Verwey, E. J. W.; Overbeek, J. T. G. *Theory of the Stability of Lyophobic Colloids*; Elsevier: Amsterdam, 1948.
(3) Guldbrand, L.; Jönsson, B.; Wennerström, H.; Linse, P. *J. Chem. Phys.* **1984**, *80*, 2221.
(4) Kjellander, R.; Marčelja, S. *J. Chem. Phys.* **1985**, *82*, 2122.
(5) Jönsson, B.; Åkesson, T.; Woodward, C. In *Ordering and Phase Transitions in Charged Colloids*; Arora, A. K., Tata, B. V. R., Eds.; VCH Publishers, 1996; Chapter 11, pp 295.
(6) Kjellander, R.; Åkesson, T.; Jönsson, B.; Marčelja, S. *J. Chem. Phys.* **1992**, *97*, 1424.
(7) Valleau, J. P.; Ivkov, R.; Torrie, G. M. *J. Chem. Phys.* **1991**, *95*, 520.
(8) Åkesson, T.; Woodward, C.; Jönsson, B. *J. Chem. Phys.* **1989**, *91*, 2461.
(9) Dahlgren, M. A. G.; Waltermo, Å.; Blomberg, E.; Claesson, P. M.; Sjöström, L.; Åkesson, T.; Jönsson, B. *J. Phys. Chem.* **1993**, *97*, 11769.
(10) Podgornik, R. *J. Phys. Chem.* **1991**, *95*, 5249.
(11) Podgornik, R. *J. Phys. Chem.* **1992**, *96*, 884.
(12) Sjöström, L.; Åkesson, T. *J. Colloid Interface Sci.* **1995**, *181*, 645.
(13) Belfort, G.; Lee, C. S. *Proc. Natl. Acad. Sci. U.S.A.* **1991**, *88*, 9146.
(14) Dahlgren, M. A. G.; Claesson, P. M.; Audebert, R. *Nordic Pulp Pap. Res. J.* **1993**, *8*, 62.
(15) Hartley, P. G.; Bailey, A. I.; Luckham, P. F.; Batts, G. *Colloids Surf.* **1993**, *77*, 191.
(16) Dahlgren, M. A. G. *J. Colloid Interface Sci.* **1996**, *181*, 654.
(17) Van der Schee, H.; Lyklema, J. *J. Phys. Chem.* **1984**, *88*, 6661.
(18) Papenhuijzen, J.; Van der Schee, H. A.; Fleer, G. J. *J. Colloid Interface Sci.* **1985**, *104*, 540.
(19) Evers, O. A.; Fleer, G. J.; Scheutjens, J. M. H. M.; Lyklema, J. *J. Colloid Interface Sci.* **1986**, *111*, 446.
(20) Böhmer, M. R.; Evers, O. A.; Scheutjens, J. M. H. M. *Macromolecules* **1990**, *23*, 2288.
(21) Fleer, G. J.; Cohen Stuart, M. A.; Scheutjens, J. M. H. M.; Cosgrove, T.; Vincent, B. *Polymers at Interfaces*, Chapman and Hall: New York, 1994.
(22) Linse, P. *Macromolecules* **1996**, *29*, 326.
(23) Granfeldt, M. K.; Miklavic, S. J.; Marčelja, S.; Woodward, C. E. *Macromolecules* **1990**, *23*, 4760.
(24) Odijk, T. *Macromolecules* **1980**, *13*, 1542.
(25) Muthutkumar, M. *J. Chem. Phys.* **1987**, *86*, 7230.
(26) Varoqui, R.; Johner, A.; Elaissari, A. *J. Chem. Phys.* **1991**, *94*, 6873.
(27) Borhukhov, I.; Andelman, D.; Orland, H. *Europhys. Lett.* **1995**, *32*, 499.
(28) Miklavic, S. J.; Woodward, C. E.; Jönsson, B.; Åkesson, T. *Macromolecules* **1990**, *23*, 4149.
(29) Woodward, C. E.; Åkesson, T.; Jönsson, B. *J. Chem. Phys.* **1994**, *101*, 2569.
(30) Miklavic, S. J.; Marčelja, S. *J. Phys. Chem.* **1988**, *92*, 6718.
(31) Misra, S.; Varanasi, S.; Varanasi, P. P. *Macromolecules* **1989**, *22*, 4173.
(32) Pincus, P. *Macromolecules* **1991**, *24*, 2912.
(33) Ross, R. S.; Pincus, P. *Macromolecules* **1992**, *25*, 2177.
(34) Zhulina, E. B.; Birshtein, T. M.; Borisov, O. V. *Macromolecules* **1995**, *28*, 1491.
(35) Hesselink, F. T. *J. Colloid Interface Sci.* **1977**, *60*, 448.
(36) Dimarzio, E. A.; McCracken, F. L. *J. Chem. Phys.* **1965**, *43*, 539.
(37) Chan, D.; Mitchell, D. J.; Ninham, B. W.; White, L. R. *J. Chem. Soc., Faraday Trans. 2* **1975**, *71*, 235.
(38) Jones, I. S.; Richmond, P. *J. Chem. Soc., Faraday Trans. 2* **1977**, *73*, 1062.

(39) Wiegel, F. W. *J. Phys. A* **1977**, *10*, 299.
(40) Furusama, K.; Kanesaka, M.; Yamashita, S. *J. Colloid Interface Sci.* **1984**, *99*, 341.
(41) Afshar-Rad, T.; Bailey, A. I.; Luckham, P. F.; MacNaughton, W.; Chapman, D. *Colloids Surf.* **1987**, *25*, 263.
(42) Wang, T. K.; Audebert, R. *J. Colloid Interface Sci.* **1988**, *121*, 32.
(43) Ennis, J.; Marčelja, S.; Kjellander, R. *Electrochim. Acta* **1996**, *41*, 2115.
(44) Ennis, J.; Kjellander, R.; Mitchell, D. J. *J. Chem. Phys.* **1995**, *102*, 975.
(45) Metropolis, N. A.; Rosenbluth, A. W.; Rosenbluth, M. N.; Teller, A.; Teller, E. *J. Chem. Phys.* **1953**, *21*, 1087.
(46) Jönsson, B.; Wennerström, H.; Halle, B. *J. Phys. Chem.* **1980**, *84*, 2179.
(47) Greberg, H.; Kjellander, R.; Åkesson, T. *Mol. Phys.* **1996**, *87*, 407.
(48) Svensson, B. R.; Woodward, C. E. *Mol. Phys.* **1988**, *64*, 247.
(49) McCormack, D.; Carnie, S. L.; Chan, D. Y. C. *J. Colloid Interface Sci.* **1995**, *169*, 177.
(50) Abramowitz, M.; Stegun, I. A. *Handbook of Mathematical Functions*; Dover: New York, 1972.